GaAs membrane PhC lasers threshold reduction using AlGaAs barriers and improved processing

Sergio Iván Flores Esparza, Aurélie Lecestre, Pascal Dubreuil, Alexandre Arnoult, Adnen Mlayah, Antoine Monmayrant, Olivier Gauthier-Lafaye

GaAs membrane PhC lasers threshold reduction using AlGaAs barriers and improved processing

Sergio Iván Flores Esparza, Aurélie Lecestre, Pascal Dubreuil, Alexandre Arnoult, Adnen Mlayah, Antoine Monmayrant, and Olivier Gauthier-Lafaye

LAAS-CNRS, Université de Toulouse, CNRS, 7 Avenue du Colonel Roche, 31400 Toulouse, France

E-mail: olivier.gauthier-lafaye@laas.fr

May 2022

Abstract. Active suspended membranes are an ideal test-bench for experimenting with novel laser geometries and principles. We show that adding thin AlGaAs barrier near the top and bottom Air/GaAs interfaces of the membrane significantly reduces the carriers non-radiative recombinations and decreases the threshold of test photonic crystal test lasers. We review the existing literature on photonic crystal membrane fabrication and propose an overview of the significant defects that can be induced by each fabrication step. Finally we propose a complete processing scheme that overcome most of these defects.

Submitted to: *Nanotechnology*

1. Introduction

2D Photonic Crystal (PhC) are particularly successful to study light-matter interaction [1, 2, 3, 4, 5, 6], induce non-linear light conversion [7, 8, 9] and to serve as extremely compact laser sources [10, 11, 12, 13, 14]. In particular, active suspended membranes are an ideal test-bench for experimenting with novel laser geometries and principles, such as chemical and biological sensors [15, 16], logic gates for photonic computation [17].

GaAs based photonic crystal membranes fabrication have been an active field of research for several years. In particular they have been used for PhC lasers and passive devices demonstrations, and are particularly attractive for Near InfraRed (NIR) active devices as efficient InGaAs Quantum Wells (QWs) or Quantum Dots (QDs). Their development has been hindered as compared to InP based lasers mostly due to the highly effective non radiative recombination rates of GaAs surfaces [18, 19], which strongly limits their practical implementation.

In this paper, we show that PhC lasers threshold can be drastically reduced by using a combination of first AlGaAs barriers that prevent carriers diffusion to the GaAs/Air interfaces, and thus reduce the carriers recombination rate, and secondly an optimized processing limiting as much as possible the plasma induced damages to the GaAs structure.

Moreover, whilst numerous bibliography references exist on GaAs etching for PhC membranes realization [20, 21, 22, 23], only a few of them deal with the various aspects of a full membrane fabrication, despite it strongly impacting the efficiency of the fabricated devices. Among these, [20] described a soft mask fabrication process for GaAs based PhC membranes showing that the steps following the PhC etching have a strong impact on the fully fabricated device aspect. In this paper, we propose an alternative full process that allows to fully remove the electrosensitive resist without N-methyl-pyrolidone (NMP) solvent and most of all without having to resort to a combination of oxidation/deoxidation wet etching of the membrane.

In the following, we will first describe the different processing steps we used for PhC membrane fabrication. In the second section we show how each step was introduced in order to minimize plasma induced defect in the membrane structure and to remove any unwanted residue from the processing. In a last section, we show that the full procedure allowed us to fabricate PhC Distributed Feedback (DFB) lasers with experimental characteristics close to the predicted ones and showing a lower threshold than using a more straightforward approach.

2. Technological process description

The investigated structure is a 270-nm-thick GaAs membrane with 3 6-nm-thick embedded $In_{0.2}Ga_{0.8}As$ quantum wells (QWs). The samples were fabricated by Molecular Beam Epitaxy on GaAs (001) substrates with a 1.5-μm-thick $Al_{0.6}Ga_{0.4}As$ sacrificial layer. As compared to structures used previously [10], described in figure 1 (a), we added 2 20-nm-thick $Al_{0.2}Ga_{0.8}As$ barriers 10-nm away from the bottom and top of the membrane layer, as shown in figure 1 (b). These additional barriers limit carrier diffusion to the top and bottom GaAs/air interfaces and prevent non-radiative recombination [24].

Figure 2 presents the process-flow that was developed in this study. The first column (Figure 2 (a)) is the reference 0_2-free process flow described below. The second and third column (Figure 2 (b) and (c)) are alternative process flow with 0_2 ashing that will help us better understand the possible damages caused by oxygen inside de membrane by studying the wet etching residues at the bottom of the surface left after hydrofluoric acid (HF) etching (dark green rocks). For e-beam lithography (green box figure 2 (a)), optimized photonic crystal DFB laser arrays, as proposed in [10] were patterned in the resist using a 20 kV electron-beam lithography tool (Raith 150) and standard CSAR-62 commercial resist (350 nm). They are exposed at an uniform dose of 90 $\mu C\,cm^{-2}$ and developed in amyl acetate for 60 s and then rinsed in isopropanol (IPA) for 60 s at room

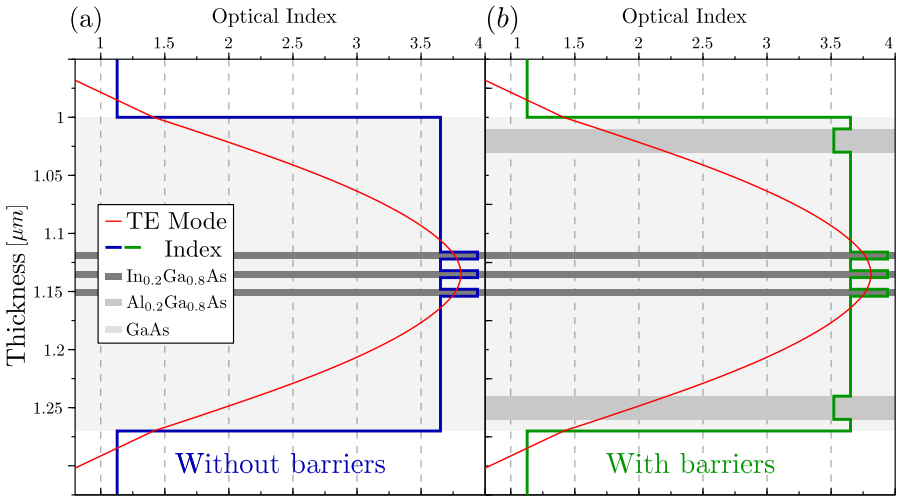

Figure 1. Comparison of membrane structures: (a) proposed in previous studies, (b) proposed in this paper. In light gray GaAs, in gray $Al_{0.2}Ga_{0.8}As$ barriers, in dark gray $In_{0.2}Ga_{0.8}As$. The TE mode profile considered is represented in red.

temperature. We then use hydrochloric acid solution for 90 s (HCl 37% mixed 1:3 by volume with deionised water (DI)) to remove oxides formed at the surface of the exposed areas.

The PhC holes are then transferred in the membrane by dry etching, more specifically inductively coupled plasma reactive ion etching (ICP-RIE) technique (Sentech Si-500) using Cl_2/N_2 chemistry [25, 26] (yellow box figure 2 (a)). Cl_2 is the main etching agent, ensuring physical etching driven by Cl ions and chemical etching driven by Cl radicals. N_2 promotes the deposition of a side-wall passivation which protects the vertical side-walls from lateral etching. We use etching parameters close to the ones of [27]: $Cl_2 = 50$ SCCM, $N_2 = 20$ SCCM, $T = 25\,^{\circ}$C, $P = 3$ mTor, duration $= 37$ s, $P_{ICP} = 200$ W and $P_{RF} = 60$ W. During the etching, samples are glued to an Si-carrier using a thermal glue (fomblin) to ensure good thermal contact between the sample and the carrier. Under these conditions we get a selectivity of around 3, which is enough to etch the holes of the photonic crystal through the 270-nm-thick membrane, while keeping a significant safety margin of CSAR62. After dry etching the remaining resist is removed using Dimethyl sulfoxide (DMSO) at a temperature of 80 °C for 2h, and then rinsed in IPA (red box figure 2 (a)). However, as can be seen in figure 3 (a) a mixture of resist and etching residues are still present, particularly around each hole of the PhC.

The next processing step is the selective wet-etching of the sacrificial layer (blue boxes figure 2 (a)). As compared to previous studies, the protocol was modified to take into account the effects of native oxidization of the bottom of the holes laying in the Al-rich sacrificial layers (figure 2 (a) dark green areas at the holes side-walls). This thin film is not etched by HF [21, 28] and therefore is left beneath the PhC hole as residues after wet-etching of the sacrificial cladding layer [22].

We use a series of several bathes with intermediate rinsing in water for 60 s, which

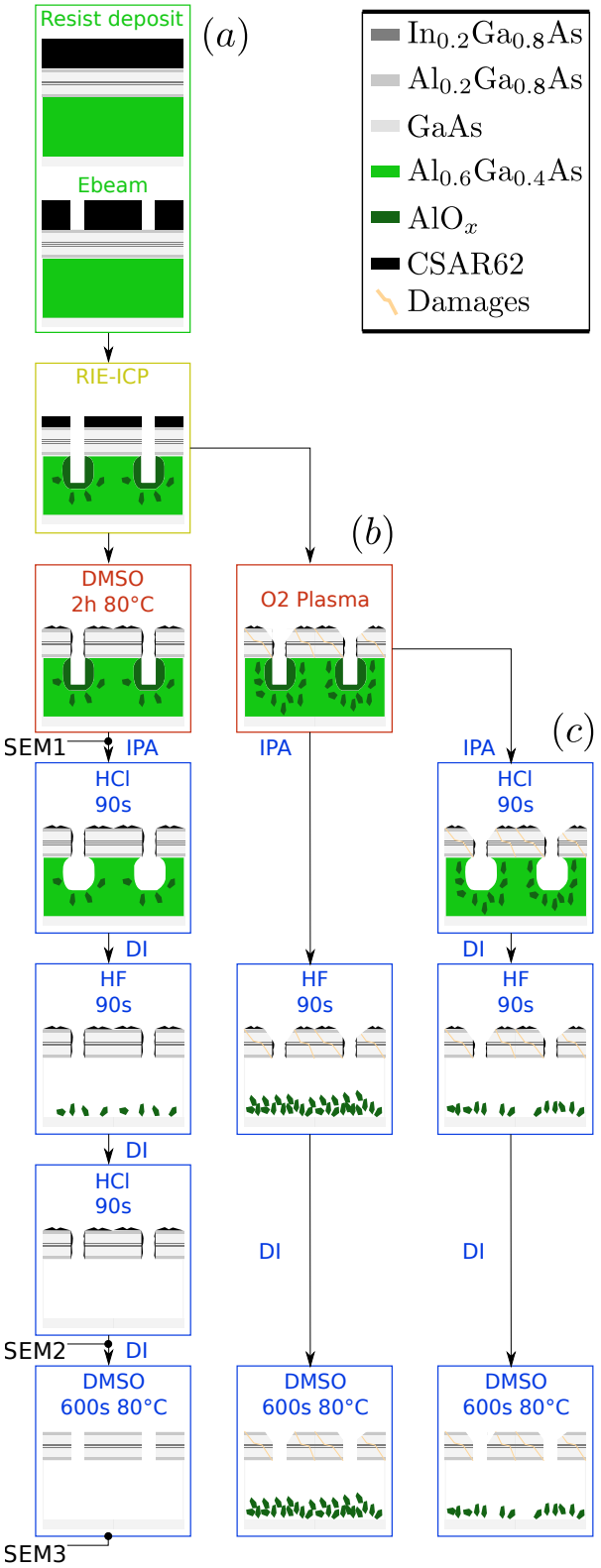

Figure 2. (a) reference process flow without 0_2 plasma; (b) & (c) two alternate process flows with 0_2 plasma ashing. Ethanol and nitrogen flow dries are not represented, but they take place after the final DMSO step.

are successively: a 300 s dip in IPA to ensure total wetting of the GaAs layers and air bubbles removal, a 90 seconds hydrochloric acid solution (HCl 37% mixed 1:3 with DI water by volume) to remove oxides formed at the surface of the sacrificial layer, specially on the side-walls of the photonic crystals (figure 2 (a) first HCl blue box) and eventually the HF sacrificial layer etching solution (HF 50% mixed 1:1 with DI water by volume) at room temperature and a magnetic stirrer for 90 s. We then proceed to a second deoxidation step by dipping the sample again in the HCl solution. This step allows to properly clean the sample from most of the residues left by wet and dry etching, specially the remaining oxides present inside the sacrificial layer (figure 2 (a) last HCl blue box: green residues are no longer present). However, as can be seen in figure 3 (b) some residues are still present around the sidewall of the holes.

The last cleaning step consists in removing the possible remaining resist by means of a DMSO solution and a stirring hot plate at a temperature of 80 °C for 600 s (figure 2 (a) DMSO blue box). As can be seen in figure 3 (c) the sample is now free from resist or etching residues.

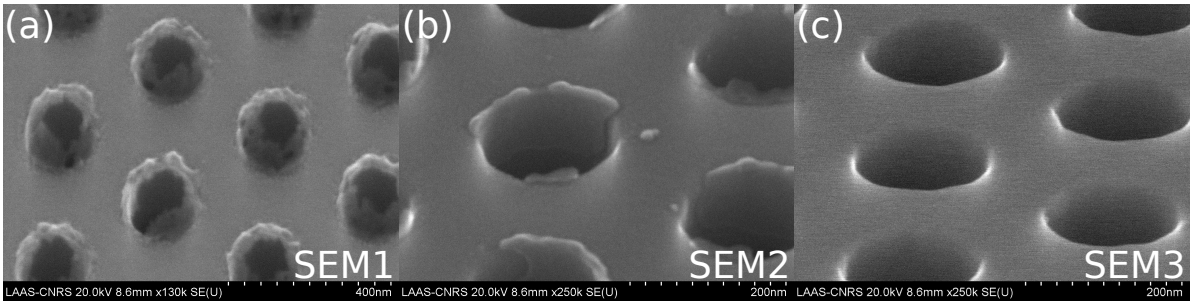

Figure 3. SEM images of PhC holes: (a) after first DMSO cleaning, (b) after wet etching but before final DMSO cleaning and (c) after final DMSO cleaning. They correspond respectively to SEM1, SEM2 and SEM3 along the process flow (a) in figure 2.

Eventually, in order to reduced the capillary forces during the drying step, we dip the sample in ethanol for 30 s before gently drying using nitrogen flow. As thin suspended GaAs membranes have moderate stiffness, capillary forces and subsequent inter-solid adhesion might lead to a collapse onto the substrate [29]. To prevent any collapse, we pay special attention to keep the entire sample under a liquid droplet during the whole process, in particular when transferring from one bath to the next.

Figure 4 shows a scanning electron microscope (SEM) image of a sample fabricated using this process. As seen in figure 4 (a) it consists of PhC waveguides of different lengths, with varying lattice constant a. Inset (b) and (c) show details of the PhC waveguide homogeneity and of the smoothness and verticality of the holes that is achieved using the previously exposed plasma parameters.

Figure 5 shows a Focussed Ion Beam Etching (FIBE) cut of a suspended PhC membrane laser. Some Gallium droplets can be seen along the edge of the cut, it is an artifact of the FIBE. The insert is a schematic representation of the suspended PhC laser.

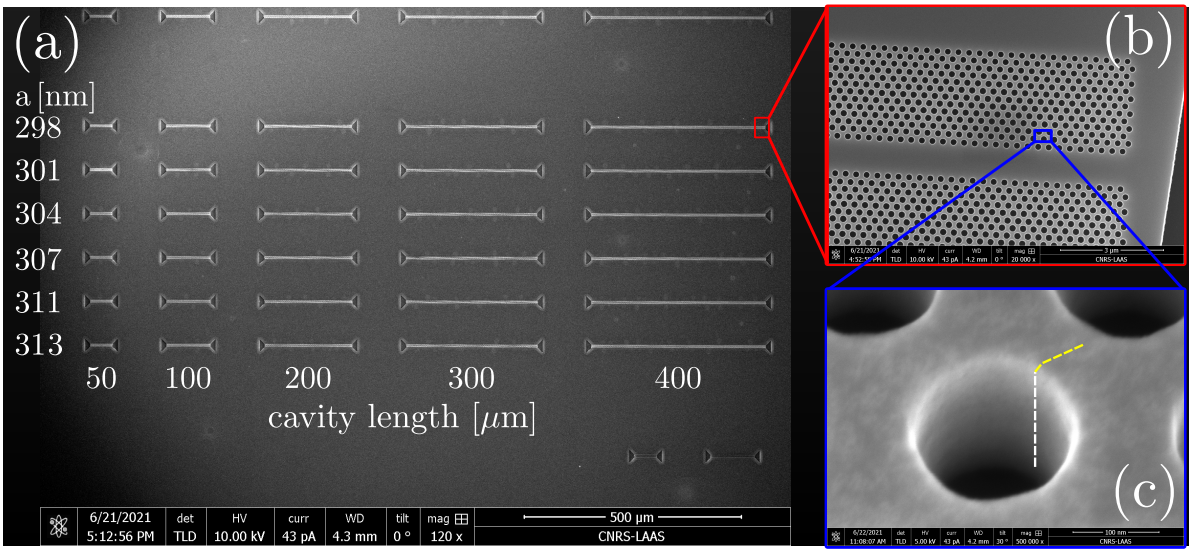

Figure 4. SEM image of the membrane DBR lasers. (a) View of the DBR lasers with increasing cavity lengths and lattice constant a. (b) Close-up on the red zone showing the homogeneity along defect waveguide in the PhC lattice. (c) Close-up on the blue zone showing the quality of the sidewall of the PhC hole. Yellow and white dashed lines are guide to the eye to appreciate hole sharpness and verticality.

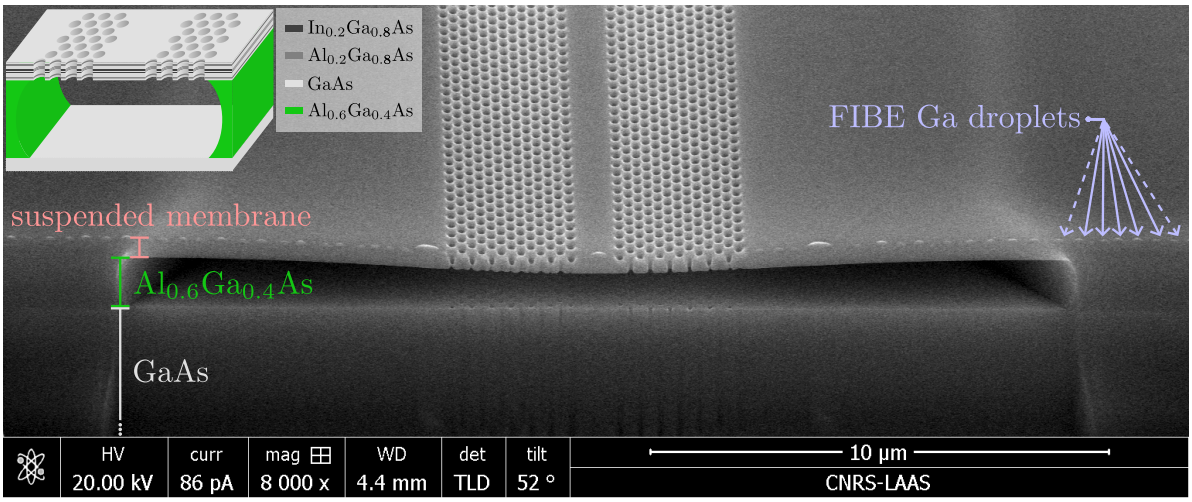

Figure 5. SEM image of the cross section of one suspended PhC membrane laser, obtained using FIBE. The insert is a schematic representation of the suspended PhC membrane laser, with the corresponding layers. The 270 nm suspended membrane is pointed out using the orange delimiter. Its composition corresponds to Figure 1 (b). The $Al_{0.6}Ga_{0.4}As$ sacrificial layer is pointed out using the green delimiter. The GaAs substrate is pointed out using the white delimiter.

3. Results and discussion

This section aims to justify the different fabrication steps of the proposed process flow. More specifically, we focus on the advantage of using organic solvent for resist striping, instead of oxygen plasma ashing. We first show the role that oxygen plasma may play

in changing the shape and size of the PhC holes. Then we show that oxygen plasma may induce damages inside the membrane and the QW despite the resist protection, therefore degrading the optoelectrical properties of the QWs [30, 31, 32], and introducing non radiative recombination sites [18, 33] enhancing losses.

3.1. Impact of oxygen plasma on hole size and shape

To highlight the impact of oxygen plasma, we prepared a sample using an alternative process flow (figure 2 (b)) where resist is stripped using O_2 plasma ashing instead of using DMSO. The ashing is carried out in the same chamber used for the dry etching (O_2 = 80 SCCM, T=25°C, P = 15 mTorr, P_{RF} = 50 W and P_{ICP}=800 W).

We monitored in-situ the resist etching using an optical reflectivity end point detection system. The resist from the large surfaces is completely etched after about 30 s of plasma ashing. We introduced different overetching times to completely remove resist from PhC holes.

Figure 6 shows a SEM image of the surface of our PhC after 46 s of O_2 plasma, before wet etching.

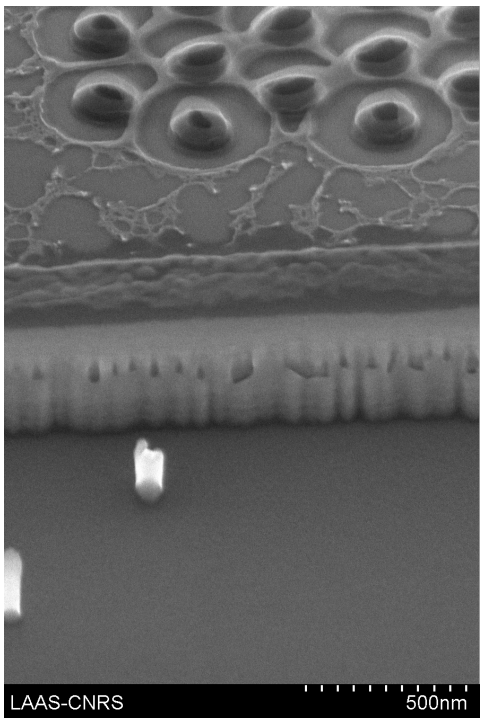

Figure 6. SEM image of PhC holes for plasma etching of 46 s, before wet etching.

Resist residues are still present, specially at the borders of the PhC holes. We did not managed to remove these residues even after dipping our sample for 48 h in acetone. This is due to resist hardening by ion bombardment during the dry etching. Other strategies for removing this residues include potassium hydroxide selective etching [21, 23] and digital etching [20, 34]. The use of potassium hydroxide

in a clean room with CMOS compatible processes requires a complex purification and neutralization process that requires dipping the sample multiple times in DI water and acetic acid. These multiple steps increase the probability of losing the surface droplet of liquid, which will result in the collapse of our suspended membrane. Moreover, KOH will slightly increase the holes diameter [20], whilst acetic acid is used in many GaAs surface preparations [35] and sometimes leads to holes geometry modifications. Concerning the second strategy, digital etching involves oxidizing the remaining resist in order to obtain volatile compounds such as CO_2 [20]. A deoxidation step is then essential in order to clean the sample from GaAs oxides. This has a direct impact on geometrical and optical properties of DFB photonic structures [1, 36] as each step reduces the membrane thickness and increases the diameter of the PhC holes.

We increased the overetching duration to try to remove all the resist, specially the one present at the borders of the PhC holes. Figure 7 (a) and (b) show SEM images of the surface of our PhC after the wet etching procedure, for two different O_2 plasma durations: 330 s and 70 s.

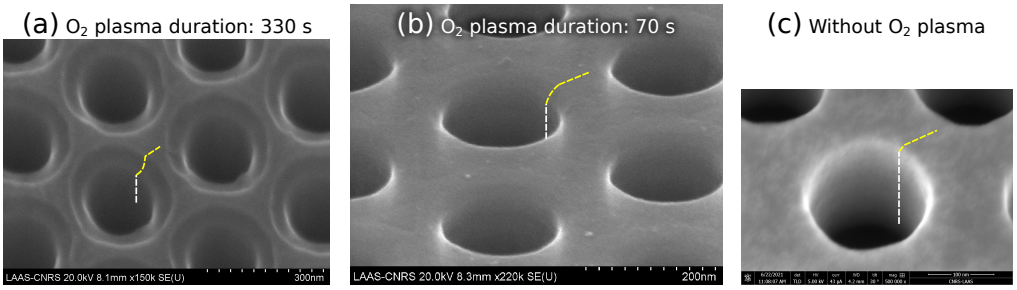

Figure 7. SEM image of PhC holes after wet etching: after (a) 330 s and (b) 70 s of O_2 plasma ashing; (c) using the O_2-free process of figure 2 (a). The vertical white dashed lines represent the intern sidewalls of the holes, the yellow dashed lines their top edge.

From figure 7 (a) and (b) we can clearly see that the top edge of the holes has a torus like form. It is easier to see, from figure 7 (a) the torus like form thanks to the contrast difference. We use white and yellow dashed lines as guides for the eye. The white dashed lines represent the vertical side-walls of the inside of the PhC holes. The yellow dashed lines the surface of the sample. The discontinuity between this dashed lines shows that the border of the holes are not vertical and are rounded, which increases their size. This effect is stronger for longer O_2 plasma (figure 7 (a)) than for shorter ones (figure 7 (b)). From figure 7 (c) we can see that this in not the case for the improved process (figure 2 (a)), as the sidewall/surface transition is sharper. In conclusion oxygen plasma over etches the top of PhC holes, affecting their size and geometry. This deviation from cylindrical hole geometry tends to increase discrepancies between expected and observed photonic properties and it hinders accurate hole diameter estimation needed to simulate the fabricated devices.

3.2. Impact of oxygen plasma on the oxidation of the membrane

In this section we discuss how oxygen plasma might introduce lattice defects and damages by implantation inside the membrane and the quantum wells [30], thus creating non radiative recombination sites [33]. This effect can be tracked by studying the composition of the residues left after the sacrificial layer etching (figure 2 (b) and (c)).

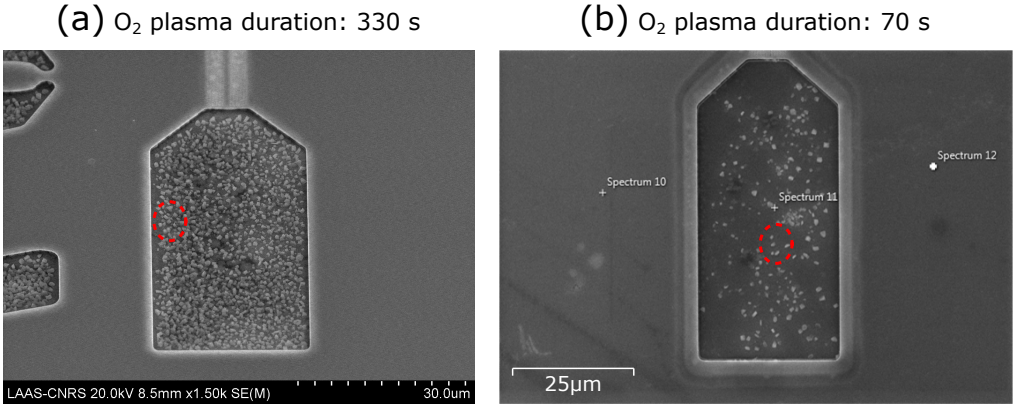

Figure 8. Scanning electron microscope (SEM) image of the bottom of the substrate after O_2 plasma ashing then wet etching of the sacrificial layer using only HF. Both samples were in contact with oxygen plasma at the same conditions as the ones showed in figure 7 (a) and (b). (a) 330 s of oxygen plasma and (b) 70 s of oxygen plasma. The red circles highlight some residues at the bottom of the substrate.

For this we use 0_2 plasma ashing for resist removal (dry etching followed by O_2 plasma instead of DMSO, processes (b) of figure 2). We then etch the sacrificial layer using only HF without any HCl treatment, as shown in figure 2 (b). The results of the wet etching of micrometric patterns are shown in figure 8 for two oxygen plasma durations: (a) 330 s and (b) 70 s. We see in figure 8 (a) a large number of rocks (dust-like gray structure covering the central part of the figure which corresponds to the bottom of the sacrificial layer). Figure 8 (b) exhibits the same rocks (dashed red circles). The density of these rocks is clearly linked to the O_2 plasma duration.

Such feature have already been observed. For example [20] observed fluoride based crystal (AlF_3). This is not the case here as these rocks do not show the crystalline characteristic form of AlF_3 and are not soluble in water, even after a rinse in H_2O for 600s.

[21, 28] pointed out the observation of an oxide compound (Al_xO_y) that comes from the aluminium-rich sacrificial layer and the contact with either O_2 plasma, residual oxygen present in the dry etching chamber, or ambient oxygen. We performed an Energy Dispersive X-Ray Analysis (EDX) to assess the presence of oxygen in the rocks.

The results from EDX are shown in figure 9. For the substrate, no oxygen line appear in the EDX spectrum (figure 9 (b)), while for rocks (figure 9 (c) and (d)), the spectra reveal the presence of oxygen (0.5 KeV). As for the compound signature of Ga- (1.098 KeV, 9.241 KeV) and As- (1.282 KeV, 10.530 KeV), we found the same intensity

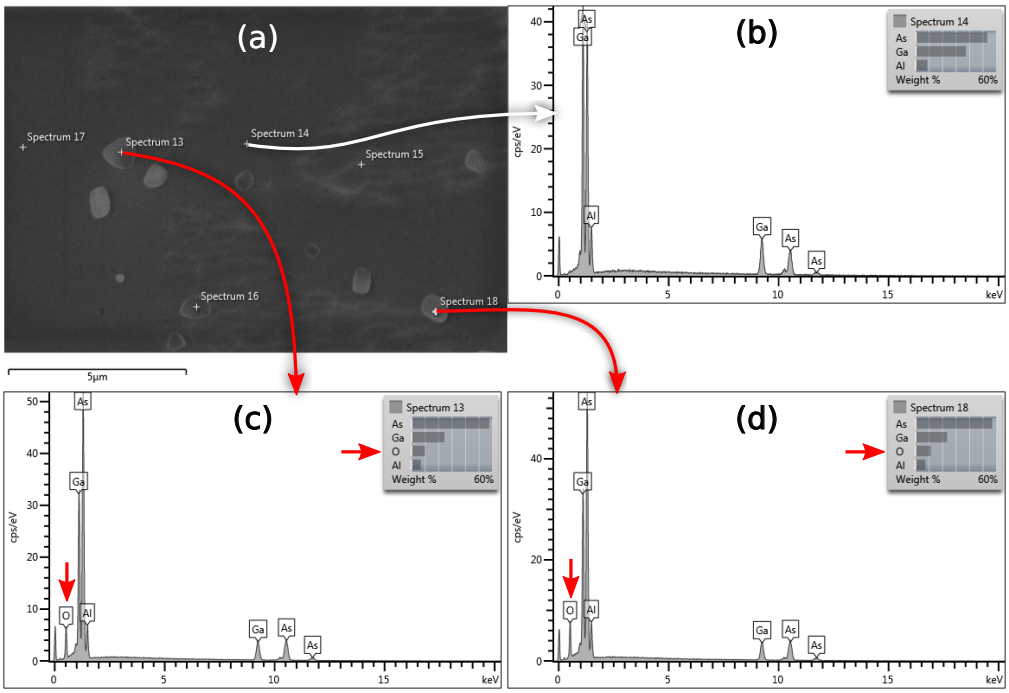

Figure 9. EDX measurements after wet etching of the sacrificial layer: SEM image of the substrate with rocks (a) ; EDX spectra of the substrate (b) and of two isolated rocks (c) and (d).

levels for rocks and the substrate. One possible explanation is that this signal comes from the interaction of the EDX ray with the substrate and not the rocks. From these EDX spectra, we conclude that the rocks contain oxygen. Moreover, as the rocks were not etched by HF, they might correspond to an Al_xO_y oxide compound.

To furthermore understand the formation of these compounds, we tested the process (c) of figure2, adding a de-oxidation after the O_2 plasma, before the sacrificial layer wet etching. If these Al_xO_y were only created on the surface of the exposed $Al_{0.6}Ga_{0.4}As$ layer, this step should allow their removal. However, surprisingly, we still found rocks, in a density increasing with the O_2 plasma duration. The sole explanation is that these Al_xO_y compounds are not only created on the exposed side-walls, but also inside the $Al_{0.6}Ga_{0.4}As$ layer. Such process are possible and have been used to demonstrate sub-surface oxidation of AlAs layers [31, 32]. It should be noted that these rocks can also be found below the PhC membranes.

In conclusion, we believe that oxygen plasma is not suited for resist removal, first because it degrades the geometry of the PhC holes, and second because it is able to implant oxygen in the semiconductor, potentially creating defects in the GaAs membrane (which is only covered by a small residual layer of resist at this stage of the process).

We thus ended with our reference dry etching procedure, as shown in figure 2 (a), for which we replace oxygen plasma with an organic solvent DMSO in order to remove the resist. DMSO was chosen for its low toxicity as compared to other solvents such as

NMP used in [20] for example.

4. Optical results

In this section we assess the impact of both the inclusion of the barrier in the vertical stack (see figure 1) and the new process without oxygen plasma (see figure 2) on the optical characteristics of the membranes.

Figure 10 shows the photoluminescence spectra of unprocessed wafers for both structures described in figure 1: in solid green for the membrane with additional barriers, in solid blue without the barrier, in dashed blue without the barrier using a $\times 20$ intensity magnification. Both spectra were recorded using identical conditions (continuous-wave, 200 mW, 532 nm excitation) and are plotted using the same arbitrary intensity units. The addition of the barriers results in a 20-fold enhancement of the luminescence, on the un-etched structure, with only a single Air/GaAs interface. Our interpretation is that the barriers prevent the optically-generated carriers to recombine non-radiatively on the top surface of the structure, and that the effect will be even stronger on the membrane.

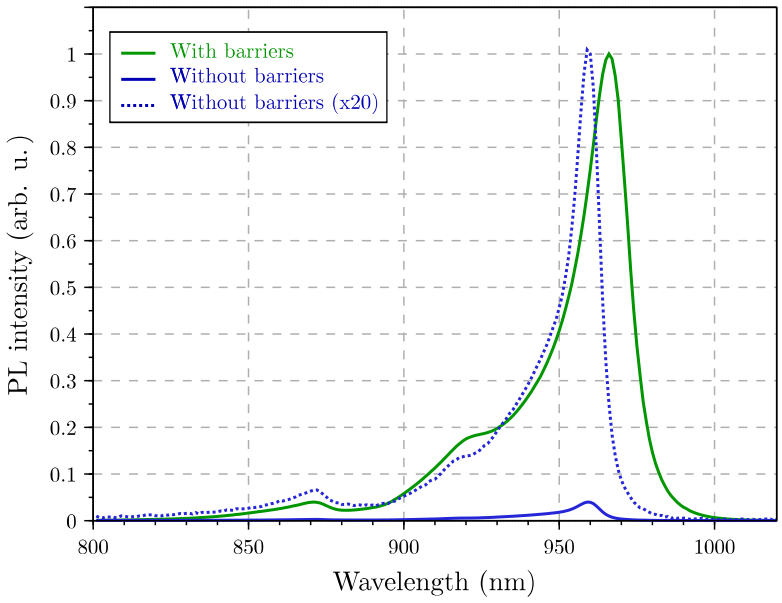

Figure 10. Photoluminescence emission from active membrane: without barriers (blue) corresponding to figure 1 (a) and with barriers (green) corresponding to figure 1 (b).

To asses the impact of both the barrier and our novel processing, we fabricated 2^{nd} order DFB lasers using an optimized deformation scheme as reported in [10]. The photonic defect waveguide acting as the DFB cavity relies on the same deformation parameters ($\alpha = 0.82$ and $\epsilon = 1.04$) and hole radius $r = 0.3\,a$ as in [10], where a is the lattice constant of the PhC.

Figure 11 (a) shows the band diagram of the considered structure (gray) together

with the fundamental mode guided in the defect (black) and the second folding point at $k_x = 0$ and $u_0 \simeq 0.312$ (yellow). We want to excite the mode at this second folding point

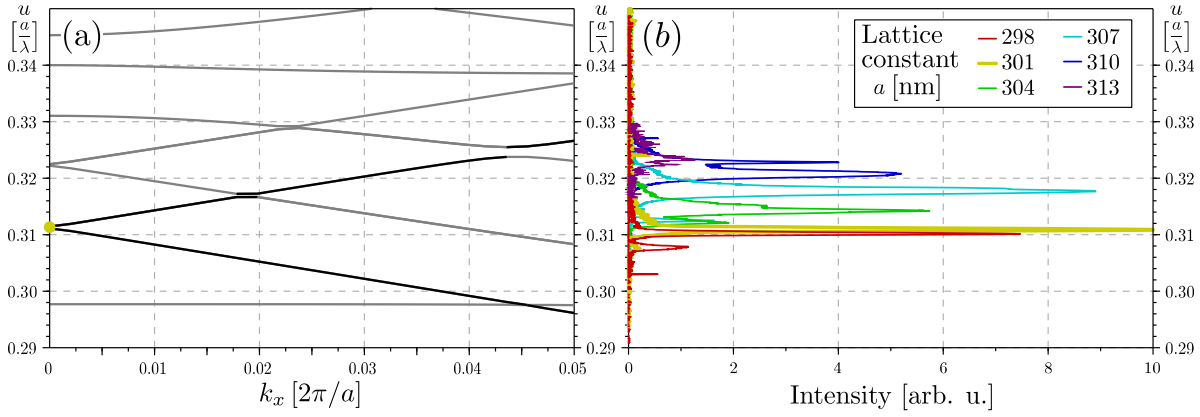

Figure 11. (a) Band diagram of the PhC waveguide (gray), fundamental guided mode (black) and DFB mode at the 2$^{\text{nd}}$ folding point (yellow). (b) Emission spectra above threshold for 300-μm-long cavities for different lattice parameters a.

where we can get efficient DFB lasing. As the gain peak in the membrane is around $\lambda_0 = 980\,\text{nm}$ this corresponds to a lattice parameter $a_0 = \lambda_0 \times u_0 \simeq 305\,\text{nm}$ and a radius $r \simeq 92\,\text{nm}$. In order to accommodate for fabrication uncertainties and dispersion in our material we fabricate DFB lasers with six different lattice parameters from $a = 298\,\text{nm}$ to $a = 313\,\text{nm}$ with a pitch of 3 nm, while keeping $r/a = 0.3$. The fabricated DFB lasers are shown in figure 4 (a), where each column corresponds to a different cavity length and each row to a different lattice parameter.

Figure 11 (b) shows the laser spectral emissions under optical pumping by an elliptical beam aligned with the waveguides for the 300-μm-long lasers, in units of a/λ, as a function of the lattice constant (colour code). We can observe two different type of emissions.

For $a = [298, 304 - 313]\,\text{nm}$, the spectrum is broad-band and contain multiple peaks. It corresponds to Fabry-Pérot laser emission for the free propagating mode guided in the defect and confined longitudinally by the etch mirrors at both ends of the waveguide.

For $a = 301\,\text{nm}$ (yellow), we observe a narrower and brighter emission corresponding the DFB mode at the second folding point. The observed experimental reduced frequency of $u = 0.311$ is in good agreement with the predicted one $u_0 \simeq 0.312$.

Figure 12 shows the emitted versus pump power curves recorded for lasers with a lattice parameter $a = 301\,\text{nm}$ and with cavity lengths of 300 μm (a) and 50 μm (b). A clear emission threshold is observed, at powers of 17 kW/cm^2 (300-μm-long cavity) and 40 kW/cm^2 (50-μm-long cavity).

The laser emission threshold of the 300-μm-long cavity is about 17 kW/cm^2, which is 8 times lower than the previously reported thresholds for such cavities ($\simeq$127 kW/cm^2) [10]. As for 50-μm-long cavity, no laser emission was possible using the membranes without barrier and the fabrication process with oxygen plasma. This is

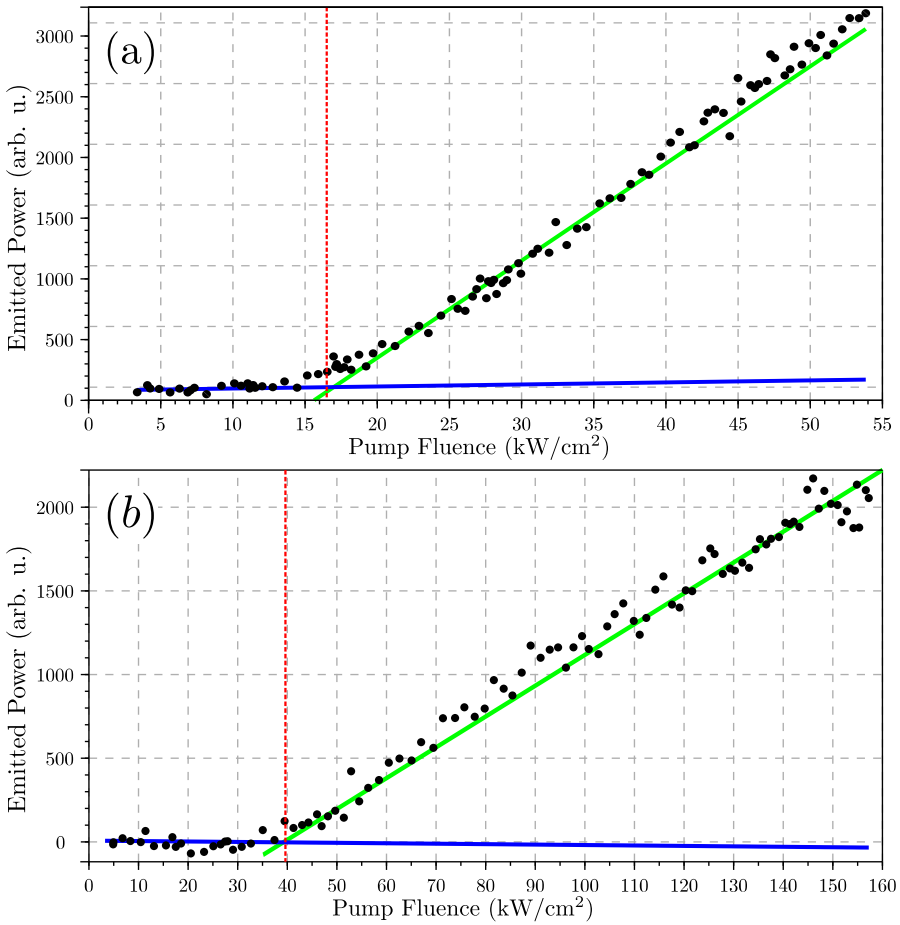

Figure 12. Emitted power versus pump fluence for (a) 300-μm and (b) 50-μm-long cavities. The red vertical dashed lines represent the laser threshold for each cavity.

a clear indication of the quality of the achieved PhC waveguides through our upgraded process, and of the impact of the AlGaAs barriers to prevent surface recombination of carriers at the GaAs/air interfaces. However, balancing the effect of the process improvement as compared to the barriers impact is difficult, and would involve a comparison between successive samples with different barriers and comparable process.

5. Conclusion

We have reviewed the complete classical fabrication process of GaAs active PhC membranes, from the epitaxial structure to the wet etching technique.

Particular attention was devoted to reducing the non-radiative recombination that occurs at the GaAs/air interfaces. For this we presented a new epitaxial structure that includes two AlGaAs barriers, near the top and bottom surface of the membrane, that significantly reduced the non-radiative recombination, rather than using chemical passivation [33, 37]. This resulted in a 20-fold enhancement of the luminescence of QWs.

On the processing side, we focused on using soft solvent-based stripping steps rather than plasma-based stripping and achieved complete cleaning of the sample together with

a good preservation of the geometrical parameters of our PhC holes.

The combination of both improvements allowed the demonstration of GaAs PhC lasers with ultra-short cavities.

6. Acknowledgements

This work was supported by LAAS-CNRS micro and nanotechnologies platform, member of the French RENATECH network. Calculations were performed using HPC resources from CALMIP (Toulouse, France) under Allocation No. 2020-P20045.

7. Bibliography

References

[1] K. Hennessy, A. Badolato, A. Tamboli, P. M. Petroff, E. Hu, M. Atatüre, J. Dreiser, and A. Imamoğlu. Tuning photonic crystal nanocavity modes by wet chemical digital etching. *Applied Physics Letters*, 87(2):021108, jul 2005.

[2] Yasutomo Ota, Masahiro Nomura, Naoto Kumagai, Katsuyuki Watanabe, Satomi Ishida, Satoshi Iwamoto, and Yasuhiko Arakawa. Enhanced photon emission and absorption of single quantum dot in resonance with two modes in photonic crystal nanocavity. *Applied Physics Letters*, 93(18):183114, nov 2008.

[3] D. G. Gevaux, A. J. Bennett, R. M. Stevenson, A. J. Shields, P. Atkinson, J. Griffiths, D. Anderson, G. A. C. Jones, and D. A. Ritchie. Enhancement and suppression of spontaneous emission by temperature tuning InAs quantum dots to photonic crystal cavities. *Applied Physics Letters*, 88(13):131101, mar 2006.

[4] Thang Ba Hoang, Johannes Beetz, Leonardo Midolo, Matthias Skacel, Matthias Lermer, Martin Kamp, Sven Höfling, Laurent Balet, Nicolas Chauvin, and Andrea Fiore. Enhanced spontaneous emission from quantum dots in short photonic crystal waveguides. *Applied Physics Letters*, 100(6):061122, feb 2012.

[5] M. Arcari, I. Söllner, A. Javadi, S. Lindskov Hansen, S. Mahmoodian, J. Liu, H. Thyrrestrup, E. H. Lee, J. D. Song, S. Stobbe, and P. Lodahl. Near-unity coupling efficiency of a quantum emitter to a photonic crystal waveguide. *Physical Review Letters*, 113(9):093603, aug 2014.

[6] K. Hennessy, A. Badolato, M. Winger, D. Gerace, M. Atatüre, S. Gulde, S. Fält, E. L. Hu, and A. Imamoğlu. Quantum nature of a strongly coupled single quantum dot–cavity system. *Nature*, 445(7130):896–899, jan 2007.

[7] Gabriel Marty, Sylvain Combrié, Fabrice Raineri, and Alfredo De Rossi. Photonic crystal optical parametric oscillator. *Nature Photonics*, 15(1):53–58, dec 2020.

[8] Ilya Fushman, Dirk Englund, Andrei Faraon, Nick Stoltz, Pierre Petroff, and Jelena Vuckovic. Controlled phase shifts with a single quantum dot. *Science*, 320(5877):769–772, may 2008.

[9] A. Javadi, I. Söllner, M. Arcari, S. Lindskov Hansen, L. Midolo, S. Mahmoodian, G Kiršanskė, T. Pregnolato, E. H. Lee, J. D. Song, S. Stobbe, and P. Lodahl. Single-photon non-linear optics with a quantum dot in a waveguide. *Nature Communications*, 6(1), oct 2015.

[10] A. Larrue, J. Campos, O. Gauthier-Lafaye, A. Monmayrant, S. Bonnefont, and F. Lozes-Dupuy. All photonic crystal DFB lasers robust toward optical feedback. *Selected Topics in Quantum Electronics, IEEE Journal of*, 17(5):1236 – 1241, 2011.

[11] X. Checoury, P. Boucaud, J-M. Lourtioz, F. Pommereau, C. Cuisin, E. Derouin, O. Drisse, L. Legouezigou, F. Lelarge, F. Poingt, G. H. Duan, D. Mulin, S. Bonnefont, O. Gauthier-Lafaye, J. Valentin, F. Lozes, and A. Talneau. Distributed feedback regime of photonic crystal waveguide lasers at 1.5μm. *Applied Physics Letters*, 85(23):5502–5504, dec 2004.

[12] X. Checoury, P. Boucaud, J.-M. Lourtioz, F. Pommereau, C. Cuisin, E. Derouin, O. Drisse, L. Legouezigou, O.L. Legouezigou, F. Lelarge, F. Poingt, Guang-Hua Duan, S. Bonnefont, D. Mulin, J. Valentin, O. Gauthier-Lafaye, F. Lozes-Dupuy, and A. Talneau. Distributed feedback-like laser emission in photonic crystal waveguides on InP substrate. *IEEE Journal of Selected Topics in Quantum Electronics*, 11(5):1180–1186, sep 2005.

[13] O. Gauthier-Lafaye, D. Mulin, S. Bonnefont, X. Checoury, J.-M. Lourtioz, A. Talneau, and F. Lozes-Dupuy. Highly monomode w1 waveguide square lattice photonic crystal lasers. *IEEE Photonics Technology Letters*, 17(8):1587–1589, aug 2005.

[14] Kuon Inoue, Hidekazu Sasaki, Koji Ishida, Yoshimasa Sugimoto, Naoki Ikeda, Yu Tanaka, Shunsuke Ohkouchi, Yusui Nakamura, and Kiyoshi Asakawa. InAs quantum-dot laser utilizing GaAs photonic-crystal line-defect waveguide. *Optics Express*, 12(22):5502, 2004.

[15] Fariborz Parandin, Farsad Heidari, Zahra Rahimi, and Saeed Olyaee. Two-dimensional photonic crystal biosensors: A review. *Optics & Laser Technology*, 144:107397, dec 2021.

[16] Rami Zegadi, Abdelouahab Zegadi, Chemseddine Zebiri, Said Mosbah, Samira Mekki, Mohamed Lamine Bouknia, and Hanane Bendjedi. Enhanced 2d photonic crystal sensor for high sensitivity sulfuric acid (h2so4) and hydrogen peroxide (h2o2) detection. *Silicon*, mar 2022.

[17] Ehsan Veisi, Mahmood Seifouri, and Saeed Olyaee. Design and numerical analysis of multifunctional photonic crystal logic gates. *Optics & Laser Technology*, 151:108068, jul 2022.

[18] D.D. Nolte. Surface recombination, free-carrier saturation, and dangling bonds in InP and GaAs. *Solid-State Electronics*, 33(2):295–298, feb 1990.

[19] Vasily N. Bessolov, Elena V. Konenkova, and Mikhail V. Lebedev. Solvent effect on the properties of sulfur passivated gaas. *Journal of Vacuum Science & Technology*

B: Microelectronics and Nanometer Structures Processing, Measurement, and Phenomena, 14(4):2761–2766, 1996.

[20] L Midolo, T Pregnolato, G Kiršanskė, and S Stobbe. Soft-mask fabrication of gallium arsenide nanomembranes for integrated quantum photonics. *Nanotechnology*, 26(48):484002, nov 2015.

[21] J. Sweet, B.C. Richards, J.D. Olitzky, J. Hendrickson, G. Khitrova, H.M. Gibbs, D. Litvinov, D. Gerthsen, D.Z. Hu, D.M. Schaadt, M. Wegener, U. Khankhoje, and A. Scherer. GaAs photonic crystal slab nanocavities: Growth, fabrication, and quality factor. *Photonics and Nanostructures - Fundamentals and Applications*, 8(1):1–6, jan 2010.

[22] Naoki Ikeda, Yoshimasa Sugimoto, Yu Tanaka, Kuon Inoue, Hisaya Oda, Yoshinori Watanabe, and Kiyoshi Asakawa. Studies on key nano-fabrication processes for GaAs-based air-bridge-type two-dimensional photonic-crystal slab waveguides. *Semiconductor Science and Technology*, 22(2):149–157, jan 2007.

[23] Pisu Jiang and Krishna C. Balram. Suspended gallium arsenide platform for building large scale photonic integrated circuits: passive devices. *Optics Express*, 28(8):12262, apr 2020.

[24] Hiroyuki Urabe, Makoto Kuramoto, Tomohiro Nakano, Atsushi Kawaharazuka, Toshiki Makimoto, and Yoshiji Horikoshi. Effects of surface barrier layer in AlGaAs/GaAs solar cells. *Journal of Crystal Growth*, 425:330–332, sep 2015.

[25] R. Braive, L. Le Gratiet, S. Guilet, G. Patriarche, A. Lemaître, A. Beveratos, I. Robert-Philip, and I. Sagnes. Inductively coupled plasma etching of GaAs suspended photonic crystal cavities. *Journal of Vacuum Science & Technology B: Microelectronics and Nanometer Structures*, 27(4):1909, 2009.

[26] Kirill A. Atlasov, Pascal Gallo, Alok Rudra, Benjamin Dwir, and Eli Kapon. Effect of sidewall passivation in bcl3 n2 inductively coupled plasma etching of two-dimensional GaAs photonic crystals. *Journal of Vacuum Science & Technology B: Microelectronics and Nanometer Structures*, 27(5):L21, 2009.

[27] Laurent Jalabert, Pascal Dubreuil, Franck Carcenac, Sébastien Pinaud, Ludovic Salvagnac, Hugues Granier, and Chantal Fontaine. High aspect ratio GaAs nanowires made by ICP-RIE etching using cl2/n2 chemistry. *Microelectronic Engineering*, 85(5-6):1173–1178, may 2008.

[28] Thor Bakke, Jan Schmidt, Martin Friedrichs, and Benjamin Völker. Etch stop materials for release by vapor hf etching. *Micromechanics Europe*, 122:68, 2005.

[29] Roya Maboudian. Critical review: Adhesion in surface micromechanical structures. *Journal of Vacuum Science & Technology B: Microelectronics and Nanometer Structures*, 15(1):1, jan 1997.

[30] P. N. Favennec. Semi-insulating layers of GaAs by oxygen implantation. *Journal of Applied Physics*, 47(6):2532–2536, jun 1976.

[31] C. Amat, G. Almuneau, P. Gallo, L. Jalabert, S. Moumdji, P. Dubreuil, T. Camps, J.B. Doucet, E. Havard, V. Bardinal, C. Fontaine, and A. Munoz-Yague. Free engineering of buried oxide patterns in GaAs/AlAs epitaxial structures. *Electronics Letters*, 43(13):730, 2007.

[32] C.S. Peng, J. Konttinen, T. Jouhti, H.F. Liu, and M. Pessa. Wet oxidation for detecting surface defect pits of AlGaAs related semiconductors. *Journal of Crystal Growth*, 274(1-2):138–143, jan 2005.

[33] F. Capasso and G. F. Williams. A proposed hydrogenation/nitridization passivation mechanism for GaAs and other III–v semiconductor devices, including InGaAs long wavelength photodetectors. *Journal of The Electrochemical Society*, 129(4):821–824, apr 1982.

[34] Gregory C. DeSalvo, Christopher A. Bozada, John L. Ebel, David C. Look, John P. Barrette, Charles L. A. Cerny, Ross W. Dettmer, James K. Gillespie, Charles K. Havasy, Thomas J. Jenkins, Kenichi Nakano, Carl I. Pettiford, Tony K. Quach, James S. Sewell, and G. David Via. Wet chemical digital etching of GaAs at room temperature. *Journal of The Electrochemical Society*, 143(11):3652–3656, nov 1996.

[35] A. R. Clawson. Guide to references on III–v semiconductor chemical etching. *Materials Science and Engineering: R: Reports*, 31(1):1–438, 2001.

[36] T. Sünner, R. Herrmann, A. Löffler, M. Kamp, and A. Forchel. Fine-tuning of GaAs photonic crystal cavities by digital etching. *Microelectronic Engineering*, 84(5-8):1405–1407, may 2007.

[37] Xianshao Zou, Chuanshuai Li, Xiaojun Su, Yuchen Liu, Daniel Finkelstein-Shapiro, Wei Zhang, and Arkady Yartsev. Carrier recombination processes in gaas wafers passivated by wet nitridation. *ACS Applied Materials & Interfaces*, 12(25):28360–28367, 2020. PMID: 32469493.